Title
Beam-energy dependence of correlations between mean transverse momentum and anisotropic flow of charged particles in Au+Au collisions at RHIC

Journal
Physics Letters B, 876

ISSN
0370-2693

Authors
Aboona, BE
Adam, J
Agakishiev, G
et al.

Publication Date
2026-05-01

DOI
10.1016/j.physletb.2026.140378

Phys. Lett. B 876 (2026) 140378

Contents lists available at ScienceDirect

Physics Letters B

journal homepage: www.elsevier.com/locate/physletb

Letter

Beam-energy dependence of correlations between mean transverse momentum and anisotropic flow of charged particles in Au + Au collisions at RHIC

The STAR Collaboration [1]

ARTICLE INFO

Editor: H Gao

Keywords:
Collectivity
Correlation
Shear viscosity
Transverse momentum correlations

ABSTRACT

The correlation between the mean transverse momentum, $[p_{\mathrm{T}}]$, and the squared anisotropic flow, v_n^2, on an event-by-event basis has been suggested to be influenced by the initial conditions in heavy-ion collisions. We present measurements of the variances and covariance of $[p_{\mathrm{T}}]$ and v_n^2, along with their dimensionless ratio, for Au + Au collisions at various beam energies: $\sqrt{s_{NN}}$ = 14.6, 19.6, 27, 54.4, and 200 GeV. Our measurements reveal a distinct energy-dependent behavior in the variances and covariances. In addition, the dimensionless ratio displays a similar behavior across different beam energies. We compare our measurements with hydrodynamic models and similar measurements from Pb + Pb collisions at the Large Hadron Collider (LHC). These findings provide valuable insights into the beam energy dependence of the specific shear viscosity (η/s) and initial-state effects, allowing for differentiating between different initial-state models.

1. Introduction

Extensive experimental measurements of heavy-ion collisions at the Relativistic Heavy Ion Collider (RHIC) [1–4] and the Large Hadron Collider [5] demonstrate the formation of the Quark-Gluon Plasma (QGP), as predicted by Quantum Chromodynamics (QCD). Many of these investigations seek to characterize the QGP's transport properties (e.g., the specific shear viscosity η/s) [6,7]. The anisotropic flow measurements, which describe the azimuthal anisotropy of the particles emitted relative to collision symmetry planes, are important in many studies [8–13]. Specifically, anisotropic flow measurements reflect the viscous hydrodynamic response to the initial spatial distribution formed in the collision at early stages [14–22].

The anisotropic flow can be characterized by the Fourier expansion [23,24] of the particle azimuthal angle (ϕ) distributions,

$$\frac{dN}{d\phi} \propto 1 + 2\sum_{n=1}^{\infty} v_n \cos\left[n(\phi - \Psi_n)\right], \tag{1}$$

where Ψ_n is the n^{th}-order flow symmetry plane. The n^{th}complex anisotropic flow vector with $v_n$magnitude and Ψ_n direction is defined as $V_n = v_n\, e^{in\Psi_n}$. The first three flow coefficients are commonly called the directed flow(v_1), the elliptic flow(v_2), and the triangular flow(v_3). Anisotropic flow measurements of the n^{th}-order flow harmonics [25–39], the correlation between different flow harmonics [40–42,42–45], and flow fluctuations [36,46–48] have led to a deeper understanding of the initial conditions of heavy-ion collisions [49,50] and the properties of the matter created in heavy-ion collisions [51,52].

Extensive comparisons between data and models across various collision energies and systems have indicated a low η/s for the QGP, yet significant uncertainties persist [8–10,16,18,53]. These uncertainties primarily arise from the difficulty in constraining the initial conditions of the collision. As a result, current theoretical and experimental investigations have sought to identify observables that could offer additional insights and tighter constraints on the initial state of heavy-ion collisions. One recent proposal is to examine the correlation between an event mean transverse momentum, $[p_{\mathrm{T}}]$, and the squared anisotropic flow, v_n^2, on an event-by-event basis [54–59]. These correlations are quantified using the Pearson correlation coefficient;

$$\rho(v_n^2, [p_T]) = \frac{\mathrm{Cov}(v_n^2, [p_T])}{\sqrt{\mathrm{Var}(v_n^2)}\sqrt{\mathrm{Var}([p_T])}}, \tag{2}$$

where, Cov(X, Y) and Var(X) represent the covariance of parameters X and Y and the variance of parameter X respectively.

The correlations between the $[p_T]$ and the v_n^2 coefficients offer valuable insights into two key aspects: (i) the relationship between the size and eccentricities in the initial state, and (ii) the correlation between the strength of the hydrodynamic response and the flow coefficients. It is noteworthy that v_n^2 ($\mathrm{Var}(v_n^2)$) is primarily influenced by eccentricities, while $[p_T]$($\mathrm{Var}([p_T])$) is driven by the transverse size of the collision zone. Specifically, events with similar energy density but smaller trans-

[1] Authors are listed at the end of this paper.

https://doi.org/10.1016/j.physletb.2026.140378
Received 18 November 2024; Received in revised form 18 February 2026; Accepted 19 March 2026
Available online 29 March 2026

verse size tend to exhibit more radial expansion, leading to larger values of $[p_T]$(Var($[p_T]$)) [60]. Furthermore, several studies [59,61–67] have highlighted the sensitivity of the $\rho(v_n^2,[p_T])$ correlation to the initial-state nuclear deformation and the nuclear geometry of the colliding nuclei.

In this letter, we use the multiparticle cumulant method to study $\rho(v_2^2,[p_T])$ and its components ($Var(v_n^2), Var([p_T])$ and $Cov(v_n^2,[p_T])$), dependence on beam energy. These measurements are expected to provide a unique data set that is comprehensive and derived from a consistent analysis across the different beam energies presented.

The Au+Au data analyzed in this study were collected by the STAR detector [68] using a minimum-bias trigger at center-of-mass energies $\sqrt{s_{NN}} = 14.6$, 19.6, 27.0, 54.4, and 200 GeV, during the years 2019, 2019, 2018, 2017, and 2011, respectively. Collision vertices were reconstructed using charged-particle tracks measured by the STAR Time Projection Chamber (TPC), which operated in a 0.5 T magnetic field aligned with the beam (z) axis [69]. Events were required to have a longitudinal vertex position, V_z, within ±30 cm for $\sqrt{s_{NN}} = 200$ GeV, ±40 cm for 54.4 and 27 GeV, and ±70 cm for 19.6 and 14.6 GeV. The transverse vertex position was constrained to $r = \sqrt{V_x^2 + V_y^2} < 2$ cm to ensure proximity to the beam axis. These vertex selection criteria were optimized for each energy to balance statistical needs with uniform detector performance: looser cuts at lower energies help maximize event yield, while tighter cuts at higher energies ensure consistent acceptance. Although such variations may influence the pseudorapidity coverage, their impact is mitigated by applying corrections as functions of V_z, centrality, η, and p_T, and by incorporating any residual effects into the systematic uncertainty estimates.

In this work, the data sets are categorized into centrality classes based on the “reference multiplicity” in the STAR experiment. This reference multiplicity is typically calculated from the raw multiplicity of primary charged particles reconstructed in the TPC across the entire azimuthal range and within $|\eta| < 0.5$. The selection of $|\eta| < 0.5$ is deliberate as it ensures a nearly uniform distribution of η in this range of the detector, and the tracks exhibit higher quality compared to those near the TPC edge. Centrality classes are established by fitting the reference multiplicity distribution to that derived from Monte Carlo Glauber simulations [70,71].

The $\rho(v_n^2,[p_T])$ correlator is derived from the covariance and variance (cf. Eq. (2)) which involve both two- and multi-particle correlations. The two- and multi-particle correlations can be influenced by nonflow effects due to resonance decays, Bose-Einstein correlations, and the fragments of individual jets [72]. The nonflow contributions can be categorized into long-range nonflow, such as the awayside jet, and short-range nonflow arising from particles emitted within a localized region in pseudorapidity, η. The latter can be effectively suppressed via sub-event cumulant methods [73–77]. In the sub-event cumulant methods, the correlated particles are taken from two or more sub-events that are separated in η. The efficiency of these methods to reduce nonflow effects has been quantified for many different two- and multi-particle correlators [22,73,74,76–78].

We construct both traditional (single-subevent, no η separation) and subevent cumulants using charged particles with $0.2 < p_T < 2.0$ GeV. To correct for detector acceptance and tracking efficiency, we apply per-particle weights following Refs.[22,73,79]. These weights depend on centrality, V_z, p_T, η, and ϕ, and incorporate the single-track efficiency. The η range of $0.35 < |\eta| < 1.0$ is selected to measure the two-particle $v_n\{2\}$ and the four-particle $v_2\{4\}$ using the two-subevent and traditional cumulant methods, respectively. Two subevents, A and C, are defined, where all tracks in sub-event A are required to be within $-1.0 < \eta_A < -0.35$ and all tracks in sub-event C are required to be within $0.35 < \eta_C < 1.0$. The v_n^2 dynamical variance is given as [80]:

$$\mathrm{Var}(v_n^2)_{dyn} = v_n\{2\}^4 - v_n\{4\}^4 = c_n^2\{2\} - c_n\{4\}. \tag{3}$$

It is important to note that, for the case of $n = 3$, the four-particle cumulant $c_3\{4\}$ is found to be approximately zero at RHIC [81]. The two-particle flow harmonics $v_n\{2\}$ can be given as:

$$c_n\{2\} = \langle\langle 2_n\rangle\rangle|_{AC} = \langle\langle e^{i\,n(\varphi^A-\varphi^C)}\rangle\rangle,$$
$$v_n\{2\} = \sqrt{c_n\{2\}}, \tag{4}$$

where $\varphi_{A(C)}$ is the azimuthal angle of particles in the region $A(C)$ and $\langle\langle 2_n\rangle\rangle$ is the two particle correlations of order n. In addition, the four-particle flow harmonic $v_2\{4\}$ can be given as:

$$c_2\{4\} = \langle\langle 4_2\rangle\rangle - 2\langle\langle 2_2\rangle\rangle^2 = \langle\langle e^{i\,2(\varphi_1+\varphi_2-\varphi_3-\varphi_4)}\rangle\rangle - 2\,\langle\langle e^{i\,2(\varphi_1-\varphi_2)}\rangle\rangle, \tag{5}$$

$$v_2\{4\} = \sqrt[4]{-c_2\{4\}}, \tag{6}$$

where $\langle\langle 4_2\rangle\rangle$ is the four particle correlations of order 2.

The dynamical p_T correlations (C_k) [55,82,83] in region B ($|\eta_B| < 0.35$) are defined as:

$$C_k = \langle \frac{1}{N_{\text{pair}}} \sum_b \sum_{b'\neq b} (p_{T,b} - \langle[p_T]\rangle)(p_{T,b'} - \langle[p_T]\rangle)\rangle, \tag{7}$$

where $\langle\rangle$ denotes an average over all events, and the two particles b and b' are required to be separated by an η gap $|\Delta\eta| > 0.2$ to suppress short-range correlations, particularly from particle/resonance decays, that can contribute to $[p_T]$ and C_k. The coefficients C_k, as defined in Eq. (7), encapsulate the event-by-event nature of (p_T) fluctuations. The event mean p_T, $[p_T]$, is given as,

$$[p_T] = \sum_{i=1}^{M_B} p_{T,i}/M_B, \tag{8}$$

where M_B is the event multiplicity in sub-event B. It is important to note that $[p_T]$ is measured within the same η range used to define centrality. The potential impact of this overlap on the measured $[p_T]$ will be systematically explored in future studies. The covariance between v_n^2 and $[p_T]$, Cov($v_n^2,[p_T]$), is defined using the three-subevents method [77,84] as,

$$\mathrm{Cov}(v_n^2,[p_T]) = \left\langle \langle 2_n\rangle|_{AC} \left([p_T] - \langle[p_T]\rangle\right)_B \right\rangle. \tag{9}$$

The resulting $\rho(v_2^2,[p_T])$ correlator [54–59,85], is obtained via Eqs. (3), (7) and (9):

$$\rho(v_n^2,[p_T]) = \frac{\mathrm{Cov}(v_n^2,[p_T])}{\sqrt{\mathrm{Var}(v_n^2)_{dyn}\; C_k}}. \tag{10}$$

The presented measurement's systematic uncertainties are evaluated from variations in the analysis cuts for event selection, track selection, and nonflow suppression. (i) The systematic errors due to the event selection were obtained by modifying the vertex selection criteria to require the vertex position to be in either the positive or negative half of the allowed region along the beam. (ii) Track selection was varied by (a) reducing the distance of the closest approach (DCA) between a track and the primary vertex from its nominal value of 3 cm to 2 cm and (b) increasing the number of TPC space points used from more than 15 points to more than 20 points (out of a maximum of 45 space points per track in the STAR TPC). (iii) The pseudorapidity gap, $\Delta\eta = \eta_1 - \eta_2$ for the track pairs, used to reduce the nonflow effects due to resonance decays, Bose-Einstein correlations, and the fragments of individual jets, was varied from $\Delta\eta = 0.7$ to $\Delta\eta = 0.9$. The overall systematic uncertainty, assuming independent sources, was taken to be the quadrature sum of the uncertainties resulting from the respective cut variations. The systematic uncertainties depend on both beam energy and collision centrality, and vary from 5% to 9%. The $\Delta\eta$ variation is the dominant source of systematic uncertainty.

The comprehensive beam energy measurements reported in this paper will help theoretical models constrain their initial conditions and better estimate how η/s varies with baryon chemical potential and temperature. Hence, it is instructive to compare our measurements to available theoretical predictions. In this work, our measurements at

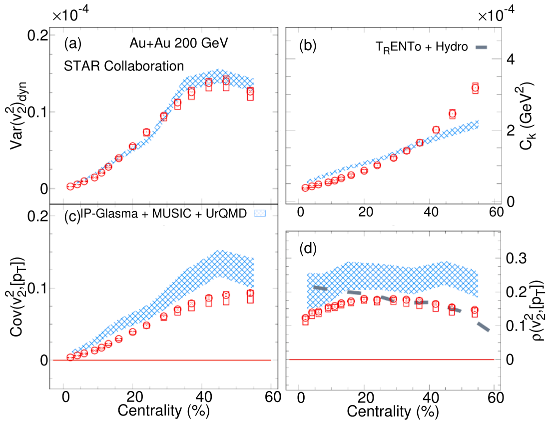

Fig. 1. Comparison of the centrality dependence of (a) $\mathrm{Var}(v_2^2)_{dyn}$, (b) C_k, (c) $\mathrm{Cov}(v_2^2,[p_T])$, and (d) $\rho(v_2^2,[p_T])$, for Au+Au collisions at $\sqrt{s_{NN}}=$ 200 GeV. Measurements are compared to theoretical calculations represented as hatched bands [86] and dashed curve [87].

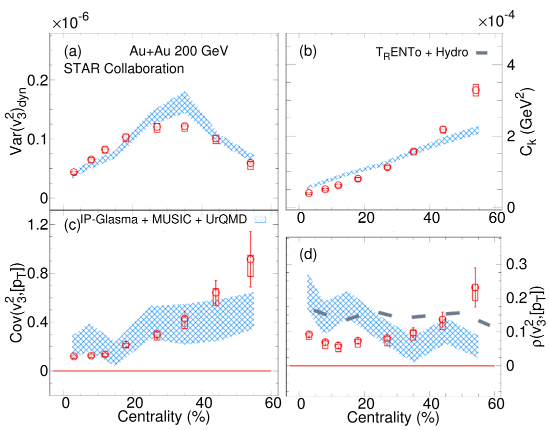

Fig. 2. Comparison of the centrality dependence of (a) $\mathrm{Var}(v_3^2)_{dyn}$, (b) C_k, (c) $\mathrm{Cov}(v_3^2,[p_T])$, and (d) $\rho(v_3^2,[p_T])$, for Au+Au collisions at $\sqrt{s_{NN}}=$ 200 GeV. Measurements are compared to theoretical calculations represented as hatched bands [86] and dashed curve [87].

$\sqrt{s_{NN}}=$ 200 GeV are compared to two theoretical models: (i) The IP-Glasma + (3+1)D MUSIC + UrQMD model [56,86], which utilizes an initial state generated from the IP-Glasma framework, followed by the MUSIC viscous hydrodynamic model with η/s of 0.12, and the UrQMD afterburner. (ii) The Trento+Hydro model [87], which employs initial conditions from the T$_R$ENTo model with a viscous hydrodynamic model with η/s of 0.05. In both models, the η/s value selection was chosen to reproduce the experimental measurements of the anisotropic flow and particle spectra.

Fig. 1 shows the centrality dependence of (a) $\mathrm{Var}(v_2^2)_{\mathrm{dyn}}$, (b) C_k, (c) $\mathrm{Cov}(v_2^2,[p_T])$, and (d) $\rho(v_2^2,[p_T])$ for Au+Au at $\sqrt{s_{NN}}=$200 GeV. The shaded bands in panels (a)–(d) denote viscous hydrodynamic predictions from IP-Glasma + MUSIC + UrQMD [86], and the dashed curve in panel (d) shows a hydrodynamic calculation with T$_R$ENTo initial conditions [87]. The IP-Glasma+MUSIC+UrQMD calculation to a good degree describes $\mathrm{Var}(v_2^2)_{\mathrm{dyn}}$ and C_k, but overpredicts $\mathrm{Cov}(v_2^2,[p_T])$ and $\rho(v_2^2,[p_T])$. For $\rho(v_2^2,[p_T])$, the T$_R$ENTo calculation agrees with the data for centralities $\gtrsim$ 20%, but overpredicts in the 0–20% most central collisions, where it is consistent with the MUSIC-based prediction. The differing magnitudes and trends underscore the constraining power of $\rho(v_2^2,[p_T])$ on theoretical models and motivate more detailed data–model comparisons in future work.

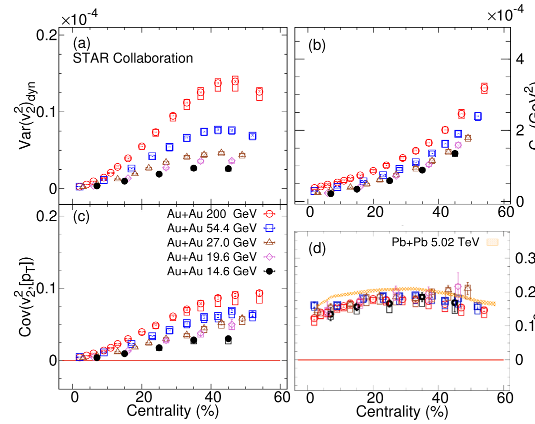

Fig. 3. Comparison of the centrality dependence of (a) $\mathrm{Var}(v_2^2)_{dyn}$, (b) C_k, (c) $\mathrm{Cov}(v_2^2,[p_T])$, and (d) $\rho(v_2^2,[p_T])$, for Au+Au collisions at $\sqrt{s_{NN}}=$ 200, 54.4, 27, 19.6, and 14.6 GeV. The curve represents the LHC measurements [94].

Fig. 2 shows the centrality dependence of the $\mathrm{Var}(v_3^2)_{dyn}$ (a), C_k (b), $\mathrm{Cov}(v_3^2,[p_T])$ (c), and $\rho(v_3^2,[p_T])$ (d) for Au+Au at $\sqrt{s_{NN}}=$ 200 GeV. The shaded bands in panels (a)–(d) and the dashed curve in panel (d) show the viscous hydrodynamic calculations of the presented quantities [86,87]. The theoretical calculations [86] show reasonable agreement with the $\mathrm{Var}(v_3^2)_{dyn}$, C_k, and the $\mathrm{Cov}(v_3^2,[p_T])$, however, they over predicts the $\rho(v_3^2,[p_T])$ measurements in central collisions.

The comparison between data and model calculations in Figs. 1 and 2 shows that, while current models provide a reasonable description of $\mathrm{Var}(v_n^2)$dyn, they tend to overestimate the values of $\rho(v_n^2,[p_T])$ in central collisions, especially for $n=3$. This discrepancy suggests that the existing models may be missing key dynamical ingredients or correlations that become increasingly important in the most central events. These results highlight the need for further theoretical developments to improve the modeling of the interplay between flow fluctuations and transverse momentum dynamics. More broadly, they underscore the power of these measurements to provide stringent constraints on theoretical frameworks, extending their impact beyond the conventional description of v_n.

Studying the beam energy dependence of the observables presented in this work offers a valuable opportunity to disentangle medium properties from initial-state effects in heavy-ion collisions [56,62,88–90]. The analysis incorporates both single-component observables, $\mathrm{Var}(v_n^2)_{\mathrm{dyn}}$, $\mathrm{Var}([p_T])$, and $\mathrm{Cov}(v_n^2,[p_T])$, as well as dimensionless correlation measures such as $\rho(v_n^2,[p_T])$. Previous investigations have shown that single-variable observables are sensitive to the interplay between initial- and final-state effects, which are expected to evolve with beam energy due to changes in the medium's temperature, density, and lifetime. In contrast, dimensionless observables like $\rho(v_n^2,[p_T])$ have been proposed as more direct probes of the initial-state geometry and its event-by-event fluctuations. Model calculations indicate that these correlation measures are largely insensitive to η/s and are instead dominated by initial-state effects [54,88,91]. This separation of sensitivities provides a powerful, testable hypothesis: since prior measurements at RHIC suggest that initial-state effects change only weakly with beam energy [92], dimensionless observables should show little to no dependence on collision energy. In contrast, observables sensitive to η/s are expected to exhibit a stronger dependence on beam energy, reflecting changes in the system's dynamical evolution. By measuring both classes of observables across a range of beam energies, this study aims to test these expectations and to provide new insights into the interplay between initial-state effects and medium transport properties. Ultimately, this combined analysis serves to validate the assumed sensitivity hierarchies and supports a more comprehensive understanding of the system created in heavy-ion collisions.

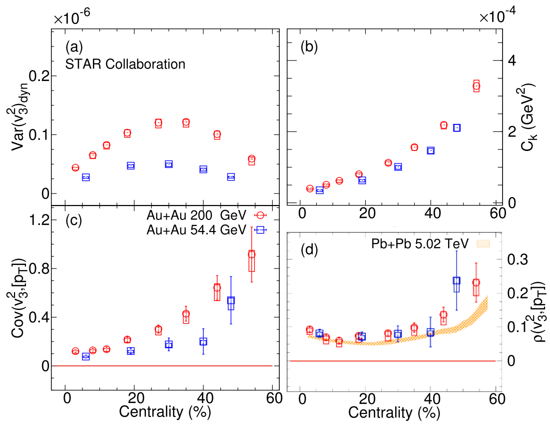

Fig. 4. The centrality dependence of the $\mathrm{Var}(v_3^2)_{dyn}$ (a), C_k (b), $\mathrm{Cov}(v_3^2,[p_T])$ (c), and $\rho(v_3^2,[p_T])$ (d), for Au+Au collisions at $\sqrt{s_{NN}}$ = 200 and 54.4 GeV. The curve represents the LHC measurements [94].

Fig. 3 shows the centrality dependence of $\mathrm{Var}(v_2^2)_{dyn}$ (a), C_k (b), $\mathrm{Cov}(v_2^2,[p_T])$ (c), and $\rho(v_2^2,[p_T])$ (d) at five different beam energies. The measurements in panels (a)–(c) show that the magnitudes of $\mathrm{Var}(v_2^2)_{dyn}$, C_k, and $\mathrm{Cov}(v_2^2,[p_T])$ decreases with beam energy over the full centrality range. Such behavior would reflect the beam energy dependence of the final state effect, given that the initial state is not a strong function of beam energy [88,89,92,93]. In contrast, the values for $\rho(v_2^2,[p_T])$ panel (d) show weak beam energy dependence. The $\rho(v^22,[pT])$ measurements are compared to published LHC results at $\sqrt{s_{\mathrm{NN}}}$ = 5.02 TeV [94]. A small difference is observed between the two measurements, which may be caused by variations in centrality definitions, mean transverse momentum, and track selection criteria (e.g., p_T and η cuts) between the two experiments. A detailed, matched-condition comparison is beyond the scope of this work, which focuses on RHIC energies with selections optimized for statistical precision in the RHIC data. Nonetheless, the overall consistency supports a largely energy-independent behavior of $\rho(v_2^2,[pT])$ within current uncertainties.

The centrality and beam-energy dependence of $\mathrm{Var}(v_3^2)_{dyn}$ (a), C_k (b), $\mathrm{Cov}(v_3^2,[p_T])$ (c), and $\rho(v_3^2,[p_T])$ (d) are presented in Fig. 4. Our presented measurements in Fig. 4 are shown at high energies (i.e., $\sqrt{s_{NN}}$ = 200 and 54.4 GeV) due to statistical limitations at lower energies. The $\rho(v_3^2,[p_T])$ panel (d) are compared to similar LHC measurements [94]. Similar to the measurements in Fig. 3, the magnitudes of $\mathrm{Var}(v_3^2)_{dyn}$ and $\mathrm{Cov}(v_3^2,[p_T])$ decrease with beam energy. In contrast, the $\rho(v_3^2,[p_T])$ panel (d) shows weak, if any, beam energy dependence. The $\rho(v_3^2,[pT])$ measurements are also compared to corresponding LHC results [94], showing good agreement and reinforcing the consistency of this observable across collision energies.

In summary, we present a comprehensive analysis of event-by-event correlations between mean transverse momentum and squared anisotropic flow coefficients in Au+Au collisions across a broad range of beam energies ($\sqrt{s_{NN}}$ = 14.6–200 GeV) using the STAR detector at RHIC. Our study examines both single-component observables, such as $\mathrm{Var}(v_n^2)_{\mathrm{dyn}}$, $\mathrm{Var}([p_T])$, and $\mathrm{Cov}(v_n^2,[p_T])$, and the dimensionless correlation measure $\rho(v_n^2,[p_T])$ for $n = 2, 3$, motivated by theoretical expectations of their different sensitivities to initial- and final-state effects. The results show a clear beam energy dependence for the single-component observables, consistent with changes in the medium's dynamics, while $\rho(v_n^2,[p_T])$ remains nearly independent of energy, reflecting its sensitivity to initial-state geometry. Comparisons to leading theoretical models reveal reasonable agreement for the single-component observables but a consistent overprediction of $\rho(v_n^2,[p_T])$, especially in central collisions, indicating that current models may be missing key dynamical features. Collectively, these findings validate the proposed separation in sensitivity between initial- and final-state effects, provide new constraints for theoretical modeling, and highlight the value of combined observables in advancing our understanding of the quark-gluon plasma created in heavy-ion collisions at RHIC.

Data availability

Data will be made available on request.

Declaration of competing interest

The authors declare that they have no known competing financial interests or personal relationships that could have appeared to influence the work reported in this paper.

Acknowledgements

We thank the RHIC Operations Group and SDCC at BNL, the NERSC Center at LBNL, and the Open Science Grid consortium for providing resources and support. This work was supported in part by the Office of Nuclear Physics within the U.S. DOE Office of Science, the U.S. National Science Foundation, National Natural Science Foundation of China, Chinese Academy of Science, the Ministry of Science and Technology of China and the Chinese Ministry of Education, NSTC Taipei, the National Research Foundation of Korea, Czech Science Foundation and Ministry of Education, Youth and Sports of the Czech Republic, Hungarian National Research, Development and Innovation Office, New National Excellency Programme of the Hungarian Ministry of Human Capacities, Department of Atomic Energy and Department of Science and Technology of the Government of India, the National Science Centre and WUT ID-UB of Poland, German Bundesministerium für Bildung, Wissenschaft, Forschung and Technologie (BMBF), Helmholtz Association, Ministry of Education, Culture, Sports, Science, and Technology (MEXT), Japan Society for the Promotion of Science (JSPS), and Agencia Nacional de Investigacion y Desarrollo de Chile (ANID), Chile.

The STAR Collaboration

B. E. Aboona[59], J. Adam[17], G. Agakishiev[32], I. Aggarwal[45], M. M. Aggarwal[45], Z. Ahammed[66], A. Aitbayev[32], I. Alekseev[3,41], E. Alpatov[41], A. K. Alshammri[33], A. Aparin[32], S. Aslam[21], J. Atchison[2], G. S. Averichev[32], V. Bairathi[57], X. Bao[53], P. Barik[26], K. Barish[12], S. Behera[27], P. Bhagat[31], A. Bhasin[31], S. Bhatta[56], I. G. Bordyuzhin[3], J. D. Brandenburg[44], A. V. Brandin[41], C. Broodo[24], X. Z. Cai[54], H. Caines[70], M. Calderón De La Barca Sánchez[10], D. Cebra[10], J. Ceska[17], I. Chakaberia[36], Y. S. Chang[47], Z. Chang[29], A. Chatterjee[18], D. Chen[12], J. H. Chen[21], L. Chen[13], Q. Chen[22], W. Chen[21], Z. Chen[53], J. Cheng[62], Y. Cheng[11], W. Christie[7], X. Chu[7], S. Corey[44], H. J. Crawford[9], G. Dale-Gau[17], A. Das[17], D. De Souza Lemos[7], T. G. Dedovich[32], I. M. Deppner[23], A. A. Derevschikov[46], A. Deshpande[56], A. Dhamija[45], A. Dimri[56], P. Dixit[21], X. Dong[36], J. L. Drachenberg[2], E. Duckworth[33], J. C. Dunlop[7], Y. S. El-Feky[5], J. Engelage[9], G. Eppley[48], S. Esumi[63], O. Evdokimov[14], O. Eyser[7], B. Fan[13], Y. Fang[62], R. Fatemi[34], S. Fazio[8], H. Feng[13], Y. Feng[13], E. Finch[55], Y. Fisyak[7], F. A. Flor[70], B. Fu[13], C. Fu[30], T. Fu[53], T. Gao[53], Y. Gao[21], G. Garcia[7], F. Geurts[48], A. Gibson[65], A. Giri[24], K. Gopal[27], X. Gou[53], D. Grosnick[65], A. Gu[25], J. Gu[21], A. Gupta[31], A. Hamed[5], R. J. Hamilton[70], J. Han[13], X. Han[44], M. D. Harasty[10], J. W. Harris[70], H. Harrison-Smith[34], L. B. Havener[70], X. H. He[30], Y. He[53], C. Hu[64], Q. Hu[30], Y. Hu[36], H. Huang[43,1], H. Z. Huang[11], S. L. Huang[56], T. Huang[14], Y. Huang[19], Y. Huang[30], Y. Huang[21], M. Isshiki[63], W. W. Jacobs[29], A. Jalotra[31], C. Jena[27], Y. Ji[64], J. Jia[56,7], X. Jiang[13], C. Jin[48], Y. Jin[13], N. Jindal[44], X. Ju[50], E. G. Judd[9], S. Kabana[57], D. Kalinkin[34], J. Kang[52], K. Kang[62], A. R. Kanuganti[7], D. Kapukchyan[17], K. Kauder[7], D. Keane[33], A. Kechechyan[32], M. Kesler[33], A. Khanal[68], A. Khanal[58], J. Kim[7], A. Kiselev[7], A. G. Knospe[37], L. Kochenda[41], Y. Kong[13], A. A. Korobitsin[32],

B. Korodi[44], A. Yu Kraeva[41], P. Kravtsov[41], L. Kumar[45], M. C. Labonte[10], R. Lacey[56], J. M. Landgraf[7], C. Larson[34], A. Lebedev[7], R. Lednicky[32], J. H. Lee[7], Y. H. Leung[23], C. Li[13], D. Li[50], H-S Li[47], H. Li[69], H. Li[22], H. Li[13], W. Li[48], X. Li[50], X. Li[50], Y. Li[62], Z. Li[51], Z. Li[50], X. Liang[12], T. Lin[53], Y. Lin[22], C. Liu[30], G. Liu[51], H. Liu[25], L. Liu[13], L. Liu[21], Z. Liu[21], Z. Liu[13], T. Ljubicic[48], O. Lomicky[17], E. M. Loyd[12], T. Lu[30], J. Luo[50], X. F. Luo[13], V. B. Luong[32], L. Ma[21], R. Ma[7], Y. G. Ma[21], N. Magdy[60], R. Manikandhan[24], O. Matonoha[17], K. Menduli[26], K. Mi[64], N. G. Minaev[46], B. Mohanty[42], B. Mondal[42], M. M. Mondal[38], I. Mooney[70], D. A. Morozov[46], M. I. Nagy[19], C. J. Naim[56], A. S. Nain[45], J. D. Nam[58], M. Nasim[26], H. Nasrulloh[50], E. Nedorezov[32], J. M. Nelson[9], M. Nie[53], G. Nigmatkulov[14], T. Niida[63], L. V. Nogach[46], T. Nonaka[63], G. Odyniec[36], A. Ogawa[7], S. Oh[52], V. A. Okorokov[41], K. Okubo[63], B. S. Page[7], M. Pal[58], S. Pal[17], A. Pandav[36], A. Panday[26], A. K. Pandey[67], Y. Panebratsev[32], T. Pani[49], P. Parfenov[41], A. Paul[12], S. Paul[56], C. Perkins[9], S. Ping[21], I. D. Ponce Pinto[70], M. Posik[58], E. Pottebaum[70], A. Povarov[41], S. Prodhan[27], T. L. Protzman[37], N. K. Pruthi[45], J. Putschke[68], Y. Qi[13], Z. Qin[62], H. Qiu[30], C. Racz[12], S. K. Radhakrishnan[33], A. Rana[45], R. L. Ray[61], C. W. Robertson[47], O. V. Rogachevsky[32], M. A. Rosales Aguilar[34], D. Roy[49], L. Ruan[7], A. K. Sahoo[30], N. R. Sahoo[27], H. Sako[63], S. Salur[49], S. S. Sambyal[31], E. Samigullin[3], D. T. Samuel[33], J. K. Sandhu[37], S. Sato[63], B. C. Schaefer[37], N. Schmitz[39], J. Seger[16], R. Seto[12], P. Seyboth[39], N. Shah[28], E. Shahaliev[32], P. V. Shanmuganathan[7], T. Shao[21], M. Sharma[31], N. Sharma[26], R. Sharma[27], S. R. Sharma[27], A. I. Sheikh[33], D. Shen[53], D. Y. Shen[30], K. Shen[50], S. Shi[13], Y. Shi[53], Shilpa[33], E. Shulga[7], F. Si[50], J. Singh[57], S. Singha[30], P. Sinha[27], M. J. Skoby[6,47], Y. Söhngen[23], Y. Song[70], T. D. S. Stanislaus[65], M. Strikhanov[41], Y. Su[50], X. Sun[30], Y. Sun[50], B. Surrow[58], D. N. Svirida[3], Z. W. Sweger[10], A. C. Tamis[70], A. H. Tang[7], Z. Tang[50], A. Taranenko[41], T. Tarnowsky[40], J. H. Thomas[36], A. Timofeev[32], D. Tlusty[16], M. V. Tokarev[32], D. Torres-Valladares[48], S. Trentalange[11], O. D. Tsai[11,7], C. Y. Tsang[33,7], Z. Tu[7], J. E. Tyler[59], T. Ullrich[7], D. G. Underwood[4,65], G. Van Buren[7], A. N. Vasiliev[46,41], F. Videbæk[7], S. Vokal[32], S. A. Voloshin[68], F. Wang[47], G. Wang[11], G. Wang[13], J. S. Wang[25], J. Wang[53], K. Wang[50], X. Wang[53], Y. Wang[50], Y. Wang[13], Y. Wang[62], Z. Wang[21], Z. Wang[13], Z. Wang[53], J. C. Webb[7], P. C. Weidenkaff[23], G. D. Westfall[40], H. Wieman[36], G. Wilks[14], S. W. Wissink[29], C. P. Wong[7], J. Wu[64], X. Wu[11], X. Wu[50], X. Wu[13], B. Xi[21], Y. Xiao[21], Z. G. Xiao[62], G. Xie[64], W. Xie[47], H. Xu[25], N. Xu[13], Q. H. Xu[53], X. Xu[62], Y. Xu[53], Y. Xu[21], Y. Xu[13], Y. Xu[30], Z. Xu[33], Z. Xu[4], G. Yan[53], Z. Yan[56], C. Yang[53], Q. Yang[53], S. Yang[51], Y. Yang[1,43], Z. Ye[51], Z. Ye[36], L. Yi[53], Y. Yu[53], W. Yuan[62], W. Zha[50], C. Zhang[21], D. Zhang[51], J. Zhang[53], K. Zhang[13], L. Zhang[13], S. Zhang[15], W. Zhang[51], X. Zhang[30], Y. Zhang[30], Y. Zhang[50], Y. Zhang[53], Y. Zhang[22], Z. Zhang[7], Z. Zhang[14], F. Zhao[35], J. Zhao[21], S. Zhou[13], Y. Zhou[13], C. Zhu[13], X. Zhu[62], M. Zurek[4,7], M. Zyzak[20]

Collaboration Institutes

[1] Academia Sinica, 115, Nankang, China
[2] Abilene Christian University, 79699, Abilene, Texas, USA
[3] Alikhanov Institute for Theoretical and Experimental Physics, NRC “Kurchatov Institute”, 117218, Moscow, Russia
[4] Argonne National Laboratory, 60439, Argonne, Illinois, USA
[5] American University, 11835, New Cairo, Cairo, Egypt
[6] Ball State University, 47306, Muncie, Indiana, USA
[7] Brookhaven National Laboratory, 11973, Upton, New York, USA
[8] University of Calabria & INFN-Cosenza, 87036, Rende, Italy
[9] University of California, 94720, Berkeley, California, USA
[10] University of California, 95616, Davis, California, USA
[11] University of California, 90095, Los Angeles, California, USA
[12] University of California, 92521, Riverside, California, USA
[13] Central China Normal University, 430079, Wuhan, Hubei, China
[14] University of Illinois at Chicago, 60607, Chicago, Illinois, USA
[15] Chongqing University, 401331, Chongqing, China
[16] Creighton University, 68178, Omaha, Nebraska, USA
[17] Czech Technical University in Prague FNSPE, 115 19, Prague, Czech Republic
[18] National Institute of Technology Durgapur, Durgapur, 713209, India
[19] ELTE Eötvös Loránd University, H-1117, Budapest, Hungary
[20] Frankfurt Institute for Advanced Studies FIAS, 60438, Frankfurt, Germany
[21] Fudan University, 200433, Shanghai, China
[22] Guangxi Normal University, 541004, Guilin, China
[23] University of Heidelberg, 69120, Heidelberg, Germany
[24] University of Houston, 77204, Houston, Texas, USA
[25] Huzhou University, 313000, Huzhou, Zhejiang, China
[26] Indian Institute of Science Education and Research (IISER), 760010, Berhampur, India
[27] Indian Institute of Science Education and Research (IISER) Tirupati, 517507, Tirupati, India
[28] Indian Institute Technology, 801106, Patna, Bihar, India
[29] Indiana University, 47408, Bloomington, Indiana, USA
[30] Institute of Modern Physics, Chinese Academy of Sciences, 730000, Lanzhou, Gansu, China
[31] University of Jammu, 180001, Jammu, India
[32] Joint Institute for Nuclear Research, 141 980, Dubna, Russia
[33] Kent State University, 44242, Kent, Ohio, USA
[34] University of Kentucky, 40506-0055, Lexington, Kentucky, USA
[35] Lanzhou University, 730000, Lanzhou, China
[36] Lawrence Berkeley National Laboratory, 94720, Berkeley, California, USA
[37] Lehigh University, 18015, Bethlehem, Pennsylvania, USA
[38] Lovely Professional University, Jalandhar - Delhi G.T. Road, 144411, Pagwara, Panjab, India
[39] Max-Planck-Institut für Physik, 80805, Munich, Germany
[40] Michigan State University, 48824, East Lansing, Michigan, USA
[41] National Research Nuclear University MEPhI, 115409, Moscow, Russia
[42] National Institute of Science Education and Research, HBNI, 752050, Jatni, India
[43] National Cheng Kung University, 70101, Tainan, Taiwan
[44] The Ohio State University, 43210, Columbus, Ohio, USA
[45] Panjab University, 160014, Chandigarh, India
[46] Institute of High Energy Physics, NRC “Kurchatov Institute”, 142281, Protvino, Russia
[47] Purdue University, 47907, West Lafayette, Indiana, USA
[48] Rice University, 77251, Houston, Texas, USA
[49] Rutgers University, 08854, Piscataway, New Jersey, USA
[50] University of Science and Technology of China, 230026, Hefei, Anhui, China
[51] South China Normal University, 510631, Guangzhou, Guangdong, China
[52] Sejong University, 05006, Seoul, Republic of Korea
[53] Shandong University, 266237, Qingdao, Shandong, China
[54] Shanghai Institute of Applied Physics, Chinese Academy of Sciences, 201800, Shanghai, China
[55] Southern Connecticut State University, 06515, New Haven, Connecticut, USA
[56] State University of New York, 11794, Stony Brook, New York, USA
[57] Instituto de Alta Investigacióon, Universidad de Tarapacá, 1000000, Arica, Chile
[58] Temple University, 19122, Philadelphia, Pennsylvania, USA
[59] Texas A&M University, 77843, College Station, Texax, USA
[60] Texas Southern University, 77004, Houston, Texas, USA
[61] University of Texas, 78712, Austin, Texas, USA
[62] Tsinghua University, 100084, Beijing, China
[63] University of Tsukuba, 305-8571, Tsukuba, Ibaraki, Japan

[64] University of Chinese Academy of Sciences, 101408, Beijing, China
[65] Valparaiso University, 46383, Valparaiso, Indiana, USA
[66] Variable Energy Cyclotron Centre, 700064, Kolkata, India
[67] Warsaw University of Technology, 00-661, Warsaw, Poland
[68] Wayne State University, 48201, Detroit, Michigan, USA
[69] Wuhan University of Science and Technology, 430065, Wuhan, Hubei, China
[70] Yale University, 06520, New Haven, Connecticut, USA

References

[1] J. Adams, et al., STAR, Experimental and theoretical challenges in the search for the quark gluon plasma: the STAR Collaboration's critical assessment of the evidence from RHIC collisions, Nucl. Phys. A 757 (2005) 102–183. arXiv:nucl-ex/0501009, https://doi.org/10.1016/j.nuclphysa.2005.03.085
[2] K. Adcox, et al., PHENIX, Formation of dense partonic matter in relativistic nucleus-nucleus collisions at RHIC: experimental evaluation by the PHENIX collaboration, Nucl. Phys. A 757 (2005) 184–283. arXiv:nucl-ex/0410003, https://doi.org/10.1016/j.nuclphysa.2005.03.086
[3] I. Arsene, et al., BRAHMS, Quark gluon plasma and color glass condensate at RHIC? The perspective from the BRAHMS experiment, Nucl. Phys. A 757 (2005) 1–27. arXiv:nucl-ex/0410020, https://doi.org/10.1016/j.nuclphysa.2005.02.130
[4] B.B. Back, et al., PHOBOS, The PHOBOS perspective on discoveries at RHIC, Nucl. Phys. A 757 (2005) 28–101. arXiv:nucl-ex/0410022, https://doi.org/10.1016/j.nuclphysa.2005.03.084
[5] B. Muller, J. Schukraft, B. Wyslouch, First results from Pb + Pb collisions at the LHC, Ann. Rev. Nucl. Part. Sci. 62 (2012) 361–386. arXiv:1202.3233, https://doi.org/10.1146/annurev-nucl-102711-094910
[6] E.V. Shuryak, Quark-gluon plasma and hadronic production of leptons, photons and psions, Sov. J. Nucl. Phys. 28 (1978) 408. https://doi.org/10.1016/0370-2693(78)90370-2
[7] E.V. Shuryak, Quantum chromodynamics and the theory of superdense matter, Phys. Rept. 61 (1980) 71–158. https://doi.org/10.1016/0370-1573(80)90105-2
[8] E. Shuryak, Why does the quark gluon plasma at RHIC behave as a nearly ideal fluid?, Prog. Part. Nucl. Phys. 53 (2004) 273–303. arXiv:hep-ph/0312227, https://doi.org/10.1016/j.ppnp.2004.02.025
[9] M. Luzum, P. Romatschke, Conformal relativistic viscous hydrodynamics: applications to RHIC results at $\sqrt{S_{NN}}$ = 200-GeV, Phys. Rev. C78 (2008) 034915. arXiv:0804.4015, https://doi.org/10.1103/PhysRevC.78.034915, https://doi.org/10.1103/PhysRevC.79.039903
[10] P. Bozek, Bulk and shear viscosities of matter created in relativistic heavy-ion collisions, Phys. Rev. C 81 (2010) 034909. arXiv:0911.2397, https://doi.org/10.1103/PhysRevC.81.034909
[11] P. Danielewicz, R.A. Lacey, P.B. Gossiaux, C. Pinkenburg, P. Chung, J.M. Alexander, R.L. McGrath, Disappearance of elliptic flow: a new probe for the nuclear equation of state, Phys. Rev. Lett. 81 (1998) 2438–2441. arXiv:nucl-th/9803047, https://doi.org/10.1103/PhysRevLett.81.2438
[12] U.W. Heinz, P.F. Kolb, Early thermalization at RHIC, Nucl. Phys. A702 (2002) 269–280. arXiv:hep-ph/0111075, https://doi.org/10.1016/S0375-9474(02)00714-5
[13] T. Hirano, U.W. Heinz, D. Kharzeev, R. Lacey, Y. Nara, Hadronic dissipative effects on elliptic flow in ultrarelativistic heavy-ion collisions, Phys. Lett. B636 (2006) 299–304. arXiv:nucl-th/0511046, https://doi.org/10.1016/j.physletb.2006.03.060
[14] P. Huovinen, P.F. Kolb, U.W. Heinz, P.V. Ruuskanen, S.A. Voloshin, Radial and elliptic flow at RHIC: further predictions, Phys. Lett. B503 (2001) 58–64.
[15] T. Hirano, K. Tsuda, Collective flow and two pion correlations from a relativistic hydrodynamic model with early chemical freeze out, Phys. Rev. C66 (2002) 054905. arXiv:nucl-th/0205043, https://doi.org/10.1103/PhysRevC.66.054905
[16] P. Romatschke, U. Romatschke, Viscosity information from relativistic nuclear collisions: how perfect is the fluid observed at RHIC?, Phys. Rev. Lett. 99 (2007) 172301. arXiv:0706.1522, https://doi.org/10.1103/PhysRevLett.99.172301
[17] M. Luzum, Flow fluctuations and long-range correlations: elliptic flow and beyond, J. Phys. G38 (2011) 124026. arXiv:1107.0592, https://doi.org/10.1088/0954-3899/38/12/124026
[18] H. Song, S.A. Bass, U. Heinz, T. Hirano, C. Shen, 200 A GeV Au + Au collisions serve a nearly perfect quark-gluon liquid, Phys. Rev. Lett. 106 (2011) 192301. [Erratum: Phys. Rev. Lett.109,139904(2012)]. arXiv:1011.2783, https://doi.org/10.1103/PhysRevLett.106.192301, https://doi.org/10.1103/PhysRevLett.109.139904
[19] J. Qian, U.W. Heinz, J. Liu, Mode-coupling effects in anisotropic flow in heavy-ion collisions, Phys. Rev. C93 (6) (2016) 064901. arXiv:1602.02813, https://doi.org/10.1103/PhysRevC.93.064901
[20] B. Schenke, S. Jeon, C. Gale, Anisotropic flow in $\sqrt{s}$ = 2.76 TeV Pb + Pb collisions at the LHC, Phys.Lett. B702 (2011) 59–63. arXiv:1102.0575, https://doi.org/10.1016/j.physletb.2011.06.065
[21] N. Magdy, X. Sun, Z. Ye, O. Evdokimov, R. Lacey, Investigation of the elliptic flow fluctuations of the identified particles using the a multi-phase transport model, Universe 6 (9) (2020) 146. arXiv:2009.02734, https://doi.org/10.3390/universe6090146
[22] N. Magdy, Characterizing initial- and final-state effects of relativistic nuclear collisions, Phys. Rev. C 107 (2) (2023) 024905. arXiv:2210.14091, https://doi.org/10.1103/PhysRevC.107.024905
[23] S. Voloshin, Y. Zhang, Flow study in relativistic nuclear collisions by Fourier expansion of Azimuthal particle distributions, Z. Phys. C 70 (1996) 665–672. arXiv:hep-ph/9407282, https://doi.org/10.1007/s002880050141
[24] A.M. Poskanzer, S.A. Voloshin, Methods for analyzing anisotropic flow in relativistic nuclear collisions, Phys. Rev. C58 (1998) 1671–1678. arXiv:nucl-ex/9805001, https://doi.org/10.1103/PhysRevC.58.1671
[25] B. Alver, et al., PHOBOS, System size, energy, pseudorapidity, and centrality dependence of elliptic flow, Phys. Rev. Lett. 98 (2007) 242302. arXiv:nucl-ex/0610037, https://doi.org/10.1103/PhysRevLett.98.242302
[26] C. Adler, et al., STAR, Elliptic flow from two and four particle correlations in Au + Au collisions at $\sqrt{S_{NN}}$ = 130-GeV, Phys. Rev. C 66 (2002) 034904. https://doi.org/10.1103/PhysRevC.66.034904
[27] J. Adams, et al., STAR, Azimuthal anisotropy at RHIC: the first and fourth harmonics, Phys. Rev. Lett. 92 (2004) 062301. [Erratum: Phys.Rev.Lett. 127, 069901 (2021)]. https://doi.org/10.1103/PhysRevLett.127.069901
[28] A. Adare, et al., PHENIX, Measurement of two-particle correlations with respect to second- and third-order event planes in Au + Au collisions at $\sqrt{s_{NN}}$ = 200 GeV, Phys. Rev. C 99 (5) (2019) 054903. arXiv:1803.01749, https://doi.org/10.1103/PhysRevC.99.054903
[29] K. Aamodt, et al., ALICE, Higher harmonic anisotropic flow measurements of charged particles in Pb-Pb collisions at $\sqrt{s_{NN}}$ = 2.76 TeV, Phys. Rev. Lett. 107 (2011) 032301. https://doi.org/10.1103/PhysRevLett.107.032301
[30] M. Aaboud, et al., ATLAS, Measurement of the azimuthal anisotropy of charged particles produced in $\sqrt{s_{NN}}$ = 5.02 TeV Pb + Pb collisions with the ATLAS detector, Eur. Phys. J. C 78 (12) (2018) 997. https://doi.org/10.1140/epjc/s10052-018-6468-7
[31] S. Chatrchyan, et al., CMS, Azimuthal anisotropy of charged particles at high transverse momenta in PbPb collisions at $\sqrt{s_{NN}}$ = 2.76 TeV, Phys. Rev. Lett. 109 (2012) 022301. https://doi.org/10.1103/PhysRevLett.109.022301
[32] S. Chatrchyan, et al., CMS, Measurement of the elliptic anisotropy of charged particles produced in PbPb collisions at $\sqrt{s}_{NN}$ = 2.76 TeV, Phys. Rev. C 87 (1) (2013) 014902. arXiv:1204.1409, https://doi.org/10.1103/PhysRevC.87.014902
[33] N. Magdy, Characterizing the initial- and final-state effects in isobaric collisions at energies available at the BNL relativistic heavy ion collider, Phys. Rev. C 109 (2) (2024) 024906. arXiv:2401.04083, https://doi.org/10.1103/PhysRevC.109.024906
[34] N. Magdy, Beam-energy dependence of the azimuthal anisotropic flow from RHIC, 2019. arXiv:1909.09640
[35] J. Adam, et al., STAR, Azimuthal harmonics in small and large collision systems at RHIC top energies, Phys. Rev. Lett. 122 (17) (2019) 172301. arXiv:1901.08155, https://doi.org/10.1103/PhysRevLett.122.172301
[36] N. Magdy, STAR, Collision system and beam energy dependence of anisotropic flow fluctuations, Nucl. Phys. A982 (2019) 255–258. arXiv:1807.07638, https://doi.org/10.1016/j.nuclphysa.2018.09.027
[37] N. Magdy, Beam energy dependence of the linear and mode-coupled flow harmonics using the a multi-phase transport model, Universe 9 (2) (2023) 107. arXiv:2302.10373, https://doi.org/10.3390/universe9020107
[38] L. Adamczyk, et al., STAR, Azimuthal anisotropy in Cu + Au collisions at $\sqrt{s_{NN}}$ = 200 GeV, Phys. Rev. C98 (1) (2018) 014915. arXiv:1712.01332, https://doi.org/10.1103/PhysRevC.98.014915
[39] N. Magdy, STAR, Viscous damping of anisotropic flow in 7.7 – 200 GeV Au + Au collisions, J. Phys. Conf. Ser. 779 (1) (2017) 012060. https://doi.org/10.1088/1742-6596/779/1/012060
[40] J. Adam, et al., STAR, Correlation measurements between flow harmonics in Au + Au collisions at RHIC, Phys. Lett. B783 (2018) 459–465. arXiv:1803.03876, https://doi.org/10.1016/j.physletb.2018.05.076
[41] J. Adam, et al., ALICE, Correlated event-by-event fluctuations of flow harmonics in Pb-Pb collisions at $\sqrt{s_{NN}}$ = 2.76 TeV, Phys. Rev. Lett. 117 (2016) 182301. arXiv:1604.07663, https://doi.org/10.1103/PhysRevLett.117.182301
[42] G. Aad, et al., ATLAS, Measurement of the correlation between flow harmonics of different order in lead-lead collisions at $\sqrt{s_{NN}}$ = 2.76 TeV with the ATLAS detector, Phys. Rev. C92 (3) (2015) 034903. arXiv:1504.01289, https://doi.org/10.1103/PhysRevC.92.034903
[43] Z. Qiu, U.W. Heinz, Event-by-event shape and flow fluctuations of relativistic heavy-ion collision fireballs, Phys. Rev. C84 (2011) 024911. arXiv:1104.0650, https://doi.org/10.1103/PhysRevC.84.024911
[44] A. Adare, et al., PHENIX, Measurements of higher-order flow harmonics in Au + Au collisions at $\sqrt{s_{NN}}$ = 200 GeV, Phys. Rev. Lett. 107 (2011) 252301. arXiv:1105.3928, https://doi.org/10.1103/PhysRevLett.107.252301
[45] G. Aad, et al., ATLAS, Measurement of event-plane correlations in $\sqrt{s_{NN}}$ = 2.76 TeV lead-lead collisions with the ATLAS detector, Phys. Rev. C90 (2) (2014) 024905. arXiv:1403.0489, https://doi.org/10.1103/PhysRevC.90.024905
[46] B. Alver, et al., PHOBOS, Importance of correlations and fluctuations on the initial source eccentricity in high-energy nucleus-nucleus collisions, Phys. Rev. C77 (2008) 014906. arXiv:0711.3724, https://doi.org/10.1103/PhysRevC.77.014906
[47] B. Alver, et al., PHOBOS, Non-flow correlations and elliptic flow fluctuations in gold-gold collisions at $\sqrt{s_{NN}}$ = 200 GeV, Phys. Rev. C81 (2010) 034915. arXiv:1002.0534, https://doi.org/10.1103/PhysRevC.81.034915
[48] J.-Y. Ollitrault, A.M. Poskanzer, S.A. Voloshin, Effect of flow fluctuations and nonflow on elliptic flow methods, Phys. Rev. C80 (2009) 014904. arXiv:0904.2315, https://doi.org/10.1103/PhysRevC.80.014904
[49] E. Retinskaya, M. Luzum, J.-Y. Ollitrault, Constraining models of initial conditions with elliptic and triangular flow data, Phys. Rev. C 89 (1) (2014) 014902. arXiv:1311.5339, https://doi.org/10.1103/PhysRevC.89.014902
[50] J.S. Moreland, J.E. Bernhard, S.A. Bass, Alternative ansatz to wounded nucleon and binary collision scaling in high-energy nuclear collisions, Phys. Rev. C 92 (1) (2015) 011901. arXiv:1412.4708, https://doi.org/10.1103/PhysRevC.92.011901

[51] D. Teaney, The effects of viscosity on spectra, elliptic flow, and HBT radii, Phys.Rev. C68 (2003) 034913. arXiv:nucl-th/0301099, https://doi.org/10.1103/PhysRevC.68.034913
[52] H. Song, S.A. Bass, U. Heinz, Elliptic flow in 200 A GeV Au + Au collisions and 2.76 A TeV Pb + Pb collisions: insights from viscous hydrodynamics + hadron cascade hybrid model, Phys.Rev. C83 (2011) 054912. arXiv:1103.2380, https://doi.org/10.1103/PhysRevC.83.054912, https://doi.org/10.1103/PhysRevC.87.019902
[53] C. Shen, U. Heinz, P. Huovinen, H. Song, Radial and elliptic flow in Pb + Pb collisions at the large hadron collider from viscous hydrodynamic, Phys. Rev. C 84 (2011) 044903. arXiv:1105.3226, https://doi.org/10.1103/PhysRevC.84.044903
[54] G. Giacalone, B. Schenke, C. Shen, Observable signatures of initial state momentum anisotropies in nuclear collisions, Phys. Rev. Lett. 125 (19) (2020) 192301. arXiv:2006.15721, https://doi.org/10.1103/PhysRevLett.125.192301
[55] P. Bozek, Transverse-momentum-flow correlations in relativistic heavy-ion collisions, Phys. Rev. C 93 (4) (2016) 044908. arXiv:1601.04513, https://doi.org/10.1103/PhysRevC.93.044908
[56] B. Schenke, C. Shen, D. Teaney, Transverse momentum fluctuations and their correlation with elliptic flow in nuclear collision, Phys. Rev. C 102 (3) (2020) 034905. arXiv:2004.00690, https://doi.org/10.1103/PhysRevC.102.034905
[57] G. Giacalone, F.G. Gardim, J. Noronha-Hostler, J.-Y. Ollitrault, Correlation between mean transverse momentum and anisotropic flow in heavy-ion collisions, Phys. Rev. C 103 (2) (2021) 024909. arXiv:2004.01765, https://doi.org/10.1103/PhysRevC.103.024909
[58] S.H. Lim, J.L. Nagle, Exploring origins for correlations between flow harmonics and transverse momentum in small collision systems (unambiguous ambiguity), 2021. arXiv:2103.01348
[59] Measurement of flow and transverse momentum correlations in Pb + Pb collisions at $\sqrt{s_{\mathrm{NN}}} = 5.02$ TeV and Xe + Xe collisions at $\sqrt{s_{\mathrm{NN}}} = 5.44$ TeV with the ATLAS detector, 2021.
[60] P. Bozek, W. Broniowski, Transverse-momentum fluctuations in relativistic heavy-ion collisions from event-by-event viscous hydrodynamics, Phys. Rev. C 85 (2012) 044910. arXiv:1203.1810, https://doi.org/10.1103/PhysRevC.85.044910
[61] G. Giacalone, Observing the deformation of nuclei with relativistic nuclear collisions, Phys. Rev. Lett. 124 (20) (2020a) 202301. arXiv:1910.04673, https://doi.org/10.1103/PhysRevLett.124.202301
[62] G. Giacalone, Constraining the quadrupole deformation of atomic nuclei with relativistic nuclear collisions, Phys. Rev. C 102 (2) (2020b) 024901. arXiv:2004.14463, https://doi.org/10.1103/PhysRevC.102.024901
[63] G. Giacalone, J. Jia, C. Zhang, Impact of nuclear deformation on relativistic heavy-ion collisions: assessing consistency in nuclear physics across energy scales, Phys. Rev. Lett. 127 (24) (2021) 242301. arXiv:2105.01638, https://doi.org/10.1103/PhysRevLett.127.242301
[64] N. Magdy, Impact of nuclear deformation on collective flow observables in relativistic U + U collisions, Eur. Phys. J. A 59 (3) (2023) 64. arXiv:2206.05332, https://doi.org/10.1140/epja/s10050-023-00982-0
[65] Imaging shapes of atomic nuclei in high-energy nuclear collisions, 2024. arXiv:2401.06625
[66] C. Zhang, J. Jia, J. Chen, C. Shen, L. Liu, Probing the octupole deformation of ^{238}U in high-energy nuclear collisions, 2025. arXiv:2504.15245
[67] STAR, Imaging nuclear shape through anisotropic and radial flow in high-energy heavy-ion collisions, Rept. Prog. Phys. 88 (10) (2025) 108601. arXiv:2506.17785, https://doi.org/10.1088/1361-6633/ae0fc3
[68] K.H. Ackermann, et al., STAR, STAR detector overview, Nucl. Instrum. Meth. A 499 (2003) 624–632. https://doi.org/10.1016/S0168-9002(02)01960-5
[69] M. Anderson, et al., The star time projection chamber: a unique tool for studying high multiplicity events at RHIC, Nucl. Instrum. Meth. A499 (2003) 659–678. arXiv:nucl-ex/0301015, https://doi.org/10.1016/S0168-9002(02)01964-2
[70] L. Adamczyk, et al., STAR, Inclusive charged hadron elliptic flow in Au + Au collisions at $\sqrt{s_{NN}} = 7.7$ - 39 GeV, Phys. Rev. C 86 (2012) 054908. https://doi.org/10.1103/PhysRevC.86.054908
[71] B.I. Abelev, et al., STAR, Identified particle production, azimuthal anisotropy, and interferometry measurements in Au + Au collisions at $\sqrt{S_{NN}} = 9.2$- GeV, Phys. Rev. C 81 (2010) 024911. https://doi.org/10.1103/PhysRevC.81.024911
[72] J. Jia, S. Mohapatra, Disentangling flow and nonflow correlations via Bayesian unfolding of the event-by-event distributions of harmonic coefficients in ultrarelativistic heavy-ion collisions, Phys. Rev. C 88 (1) (2013) 014907. arXiv:1304.1471, https://doi.org/10.1103/PhysRevC.88.014907
[73] J. Jia, M. Zhou, A. Trzupek, Revealing long-range multiparticle collectivity in small collision systems via subevent cumulants, Phys. Rev. C96 (3) (2017) 034906. arXiv:1701.03830, https://doi.org/10.1103/PhysRevC.96.034906
[74] P. Huo, K. Gajdošová, J. Jia, Y. Zhou, Importance of non-flow in mixed-harmonic multi-particle correlations in small collision systems, Phys. Lett. B 777 (2018) 201–206. arXiv:1710.07567, https://doi.org/10.1016/j.physletb.2017.12.035
[75] C. Zhang, J. Jia, J. Xu, Non-flow effects in three-particle mixed-harmonic azimuthal correlations in small collision systems, Phys. Lett. B792 (2019) 138–141. arXiv:1812.03536, https://doi.org/10.1016/j.physletb.2019.03.035
[76] N. Magdy, O. Evdokimov, R.A. Lacey, A method to test the coupling strength of the linear and nonlinear contributions to higher-order flow harmonics via event shape engineering, J. Phys. G 48 (2) (2020) 025101. arXiv:2002.04583, https://doi.org/10.1088/1361-6471/abcb59
[77] C. Zhang, A. Behera, S. Bhatta, J. Jia, Non-flow effects in correlation between harmonic flow and transverse momentum in nuclear collisions, 2021. arXiv:2102.05200
[78] N. Magdy, Measuring differential flow angle fluctuations in relativistic nuclear collisions, Phys. Rev. C 106 (4) (2022) 044911. arXiv:2207.04530, https://doi.org/10.1103/PhysRevC.106.044911
[79] N. Magdy, Measuring differential particle correlations in relativistic nuclear collisions, Phys. Rev. C 110 (2) (2024) 024906. arXiv:2405.19169, https://doi.org/10.1103/PhysRevC.110.024906
[80] P. Bozek, R. Samanta, Higher order cumulants of transverse momentum and harmonic flow in relativistic heavy ion collisions, Phys. Rev. C 104 (1) (2021) 014905. arXiv:2103.15338, https://doi.org/10.1103/PhysRevC.104.014905
[81] L. Adamczyk, et al., STAR, Third harmonic flow of charged particles in Au + Au collisions at sqrtsNN = 200 GeV, Phys. Rev. C 88 (1) (2013) 014904. arXiv:1301.2187, https://doi.org/10.1103/PhysRevC.88.014904
[82] B.B. Abelev, et al., ALICE, Event-by-event mean p_{T} fluctuations in pp and Pb-Pb collisions at the LHC, Eur. Phys. J. C 74 (10) (2014a) 3077. arXiv:1407.5530, https://doi.org/10.1140/epjc/s10052-014-3077-y
[83] B.B. Abelev, et al., ALICE, Event-by-event mean p_{T} fluctuations in pp and Pb-Pb collisions at the LHC, Eur. Phys. J. C 74 (10) (2014b) 3077. arXiv:1407.5530, https://doi.org/10.1140/epjc/s10052-014-3077-y
[84] G. Aad, et al., ATLAS, Measurement of flow harmonics correlations with mean transverse momentum in lead-lead and proton-lead collisions at $\sqrt{s_{NN}} = 5.02$ TeV with the ATLAS detector, Eur. Phys. J. C 79 (12) (2019) 985. arXiv:1907.05176, https://doi.org/10.1140/epjc/s10052-019-7489-6
[85] P. Bozek, H. Mehrabpour, Correlation coefficient between harmonic flow and transverse momentum in heavy-ion collisions, Phys. Rev. C 101 (6) (2020) 064902. arXiv:2002.08832, https://doi.org/10.1103/PhysRevC.101.064902
[86] B. Schenke, C. Shen, P. Tribedy, Multi-particle and charge-dependent azimuthal correlations in heavy-ion collisions at the relativistic heavy-ion collider, Phys. Rev. C 99 (4) (2019) 044908. arXiv:1901.04378, https://doi.org/10.1103/PhysRevC.99.044908
[87] P. Alba, V. Mantovani Sarti, J. Noronha, J. Noronha-Hostler, P. Parotto, I.P. Vazquez, C. Ratti, Effect of the QCD equation of state and strange hadronic resonances on multiparticle correlations in heavy ion collisions, 2017. arXiv:1711.05207
[88] N. Magdy, P. Parfenov, A. Taranenko, I. Karpenko, R.A. Lacey, Model study of the energy dependence of the correlation between anisotropic flow and the mean transverse momentum in Au + Au collisions, Phys. Rev. C 105 (4) (2022) 044901. arXiv:2111.07406, https://doi.org/10.1103/PhysRevC.105.044901
[89] N. Magdy, R.A. Lacey, Model investigations of the correlation between the mean transverse momentum and anisotropic flow in shape-engineered events, Phys. Lett. B 821 (2021) 136625. arXiv:2105.04879, https://doi.org/10.1016/j.physletb.2021.136625
[90] L. Zhang, J. Chen, C. Zhang, Energy dependence of transverse momentum fluctuations in Au + Au collisions from a multiphase transport model, Phys. Rev. C 111 (2) (2025) 024911. arXiv:2501.08209, https://doi.org/10.1103/PhysRevC.111.024911
[91] M. Virta, J. Parkkila, D.J. Kim, Enhancing Bayesian parameter estimation by adapting to multiple energy scales in heavy-ion collisions at RHIC and at the LHC, Phys. Rev. C 111 (4) (2025) 044903. arXiv:2411.01932, https://doi.org/10.1103/PhysRevC.111.044903
[92] M. Abdallah, et al., STAR, Collision-system and beam-energy dependence of anisotropic flow fluctuations, Phys. Rev. Lett. 129 (25) (2022) 252301. arXiv:2201.10365, https://doi.org/10.1103/PhysRevLett.129.252301
[93] B. Aboona, et al., STAR, Beam energy dependence of the linear and mode-coupled flow harmonics in Au + Au collisions, Phys. Lett. B 839 (2023) 137755. arXiv:2211.11637, https://doi.org/10.1016/j.physletb.2023.137755
[94] S. Acharya, et al., ALICE, Characterizing the initial conditions of heavy-ion collisions at the LHC with mean transverse momentum and anisotropic flow correlations, Phys. Lett. B 834 (2022) 137393. arXiv:2111.06106, https://doi.org/10.1016/j.physletb.2022.137393